Radiology

CT-derived Chest Muscle Metrics for Outcome Prediction in Patients with COVID-19

*Simone Schiaffino, MD** • *Domenico Albano, MD** • *Andrea Cozzi, MD* • *Carmelo Messina, MD* • *Roberto Arioli, MD* • *Claudio Bnà, MD, PhD* • *Antonio Bruno, MD* • *Luca A. Carbonaro, MD* • *Alessandro Carriero, MD* • *Serena Carriero, MD* • *Pietro S. C. Danna, MD* • *Elisa D'Ascoli, MD* • *Claudia De Berardinis, MD* • *Gianmarco Della Pepa, MD* • *Zeno Falaschi, MD* • *Salvatore Gitto, MD* • *Alexis E. Malavazos, MD, PhD* • *Giovanni Mauri, MD* • *Lorenzo Monfardini, MD* • *Alessio Paschè, MD* • *Roberto Rizzati, MD* • *Francesco Secchi, MD, PhD* • *Angelo Vanzulli, MD* • *Valeria Tombini, MD* • *Ilaria Vicentin, MD* • *Domenico Zagaria, MD* • *Francesco Sardanelli, MD* • *Luca M. Sconfienza, MD, PhD*

From the Unit of Radiology (S.S., L.A.C., F. Secchi, F. Sardanelli) and High Specialty Center for Dietetics, Nutritional Education and Cardiometabolic Prevention (A.E.M.), Istituto di Ricovero e Cura a Carattere Scientifico Policlinico San Donato, Via Rodolfo Morandi 30, 20097 San Donato Milanese, Milan, Italy; Department of Biomedicine, Neurosciences and Advanced Diagnostics, Section of Radiological Sciences, Università degli Studi di Palermo, Palermo, Italy (D.A.); Unit of Radiology, Istituto di Ricovero e Cura a Carattere Scientifico Istituto Ortopedico Galeazzi, Milan, Italy (D.A., C.M., L.M.S.); Department of Biomedical Sciences for Health (A. Cozzi, S.G., F. Secchi, F. Sardanelli, L.M.S.), Postgraduate School in Radiodiagnostics (S.C., E.D., C.D.B., G.D.P.), and Department of Oncology and Hematology-Oncology (G.M., A.V.), Università degli Studi di Milano, Milan, Italy; Division of Radiodiagnostics, Department of Diagnosis and Treatment Services, Azienda Ospedaliero Universitaria Maggiore della Carità, Novara, Italy (R.A., A. Carriero, P.S.C.D., Z.F., A.P., D.Z.); Department of Radiology, Fondazione Poliambulanza Istituto Ospedaliero, Brescia, Italy (C.B., L.M.); Department of Radiology, Ospedale Santissima Annunziata, Cento, Italy (A.B., R.R.); Department of Translational Medicine, Università degli Studi del Piemonte Orientale, Novara, Italy (A. Carriero); Division of Interventional Radiology, Istituto di Ricovero e Cura a Carattere Scientifico Istituto Europeo di Oncologia, Milan, Italy (G.M.); and Azienda Socio-Sanitaria Territoriale (ASST) Grande Ospedale Metropolitano Niguarda, Milan, Italy (A.V., V.T., I.V.). Received October 26, 2020; revision requested October 27; revision received February 19, 2021; accepted March 2. **Address correspondence to**. F.S. (e-mail: *francesco.sardanelli@unimi.it*).

This study was partially supported by Ricerca Corrente funding from the Italian Ministry of Health to IRCCS Policlinico San Donato.

* S.S. and D.A. contributed equally to this work.

Conflicts of interest are listed at the end of this article.

Radiology 2021; 300:E328–E336 • https://doi.org/10.1148/radiol.2021204141 • Content codes: CH CT

Background: Lower muscle mass is a known predictor of unfavorable outcomes, but its prognostic impact on patients with COVID-19 is unknown.

Purpose: To investigate the contribution of CT-derived muscle status in predicting clinical outcomes in patients with COVID-19.

Materials and Methods: Clinical or laboratory data and outcomes (intensive care unit [ICU] admission and death) were retrospectively retrieved for patients with reverse transcriptase polymerase chain reaction–confirmed SARS-CoV-2 infection, who underwent chest CT on admission in four hospitals in Northern Italy from February 21 to April 30, 2020. The extent and type of pulmonary involvement, mediastinal lymphadenopathy, and pleural effusion were assessed. Cross-sectional areas and attenuation by paravertebral muscles were measured on axial CT images at the T5 and T12 vertebral level. Multivariable linear and binary logistic regression, including calculation of odds ratios (ORs) with 95% CIs, were used to build four models to predict ICU admission and death, which were tested and compared by using receiver operating characteristic curve analysis.

Results: A total of 552 patients (364 men and 188 women; median age, 65 years [interquartile range, 54–75 years]) were included. In a CT-based model, lower-than-median T5 paravertebral muscle areas showed the highest ORs for ICU admission (OR, 4.8; 95% CI: 2.7, 8.5; $P < .001$) and death (OR, 2.3; 95% CI: 1.0, 2.9; $P = .03$). When clinical variables were included in the model, lower-than-median T5 paravertebral muscle areas still showed the highest ORs for both ICU admission (OR, 4.3; 95%: CI: 2.5, 7.7; $P < .001$) and death (OR, 2.3; 95% CI: 1.3, 3.7; $P = .001$). At receiver operating characteristic analysis, the CT-based model and the model including clinical variables showed the same area under the receiver operating characteristic curve (AUC) for ICU admission prediction (AUC, 0.83; $P = .38$) and were not different in terms of predicting death (AUC, 0.86 vs AUC, 0.87, respectively; $P = .28$).

Conclusion: In hospitalized patients with COVID-19, lower muscle mass on CT images was independently associated with intensive care unit admission and in-hospital mortality.

Online supplemental material is available for this article.

The clinical picture of COVID-19 includes fever, cough, dyspnea, fatigue, and myalgia, with possible evolution to severe pneumonia, acute respiratory distress syndrome, and even death (1). As suggested by recent studies, older patients and those with underlying comorbidities such as heart or lung disease, obesity, and diabetes are at higher risk of developing severe complications (1,2).

Lower muscle mass and sarcopenia (ie, progressive loss of skeletal muscle mass [SMM] and strength) are also generally encountered in older individuals (3) and are independent predictors of unfavorable outcomes in trauma, cancer, chronic disease, and major surgery (3–7). Body composition might affect the clinical outcome of patients with pneumonia, as suggested by several authors (8,9) and as proven by Buchman et al (10), who identified an independent association between mortality in patients with pneumonia and the degree of respiratory muscle and extremity muscle strength, coupled with the level of pulmonary function.

Abbreviations

AUC = area under the receiver operating characteristic curve, GGO = ground-glass opacity, ICU = intensive care unit, OR = odds ratio, SMM = skeletal muscle mass

Summary

Determining the CT-derived muscle status enabled prediction of clinical outcomes (intensive care unit admission and death during hospitalization) in patients with COVID-19.

Key Results

- At multivariable binary logistic regression in 552 patients with COVID-19 who underwent CT at emergency department admission, lower-than-median T5 paravertebral muscle areas yielded the highest significant odds ratios (ORs) for intensive care unit admission (OR, 4.3; $P < .001$) and death (OR, 2.3; $P = .001$).
- A combined model including the CT-derived muscle status and the extent of lung disease enabled prediction of death (area under the receiver operating characteristic curve, 0.81) without there being any increase in its predictive performance when clinical data were added.

Among body composition parameters, visceral fat has been extensively shown to be an adverse outcome predictor in patients with COVID-19 (11). Conversely, the postulated prognostic impact of lower muscle mass in patients with COVID-19 (12) has only been preliminarily evaluated (13,14), although it could be considered a proxy of the general health status and of the action of various typical comorbidities in older patients. If present, the exploitation of an association between muscle mass and outcomes in patients with COVID-19 would rely on prompt identification of such a status, possibly even at emergency department admission, to aid patient stratification. Of note, information on muscle status could be easily retrieved by segmentation of specific skeletal muscle districts (4,7) on images from chest CT, which has been extensively used for patients' triage and monitoring during the COVID-19 pandemic (15–20)—mainly to address the shortcomings of reverse transcriptase polymerase chain reaction testing (15,18). Compared with detailed retrieval of comorbidities through history taking and compared with extensive laboratory panel tests, chest CT could therefore enable a two-sided approach for patient triage and management planning.

Thus, in this study, we aimed to retrospectively investigate the potential contribution of the CT-derived muscle status in predicting clinical outcomes in patients with COVID-19.

Materials and Methods

This multicenter, retrospective, observational study involved four hospitals in Northern Italy: Azienda Ospedaliero Universitaria Maggiore della Carità, Novara (center 1); Azienda Socio-Sanitaria Territoriale Grande Ospedale Metropolitano Niguarda, Milano (center 2); Fondazione Poliambulanza Istituto Ospedaliero, Brescia (center 3); and Istituto di Ricovero e Cura a Carattere Scientifico Istituto Ortopedico Galeazzi, Milano (center 4). Approval from the ethics committee of each institution was obtained, and specific informed consent was waived.

Consecutive hospitalized patients with reverse transcriptase polymerase chain reaction–confirmed SARS-CoV-2 infection who underwent chest CT within 24 hours of emergency department admission were included (Fig 1). Exclusion criteria subsequently applied regarded the presence of diseases that chronically impair muscular status (eg, Duchenne dystrophy) or inadequate CT image quality (eg, presence of motion artifacts or spine implants) preventing adequate segmentation of the paravertebral skeletal muscle area. Patient-specific data at emergency department admission were retrieved from electronic records (Table E1 [online]) and included demographics, body mass index values, symptoms, comorbidities, and laboratory test results, with focus being placed on major negative clinical predictors for patients with COVID-19 (21). Clinical outcomes, such as intensive care unit (ICU) admission and discharge or death, were retrospectively retrieved.

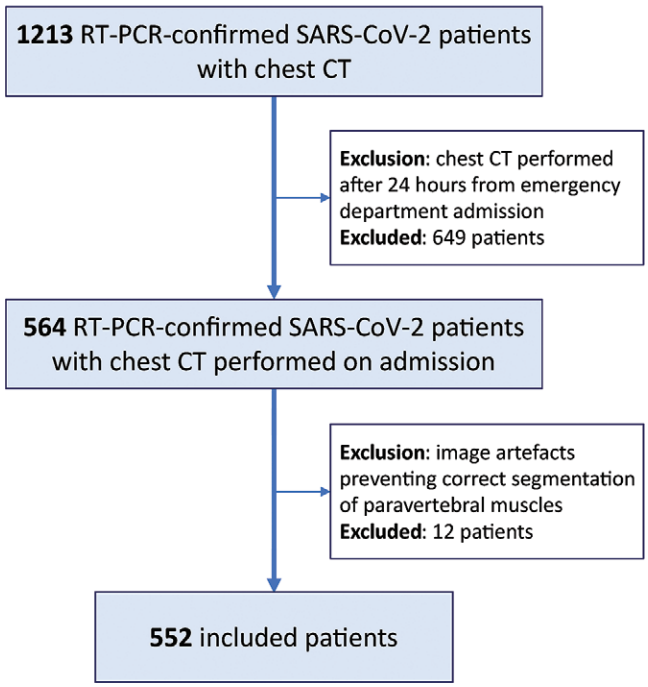

Figure 1: Flowchart of patients' enrollment. RT-PCR = reverse transcriptase polymerase chain reaction.

Image Acquisition and Analysis

All chest CT examinations were performed with the patient in a supine position and during a single inspiratory breath hold whenever possible. Technical characteristics of CT scanners and acquisition parameters for each center are listed in Table E2 (online).

Image analysis was independently performed by four radiologists (D.A., R.A., L.M., and V.T.) with 8–15 years of experience in chest imaging. The progression and extent of pulmonary parenchymal involvement were assessed by the radiologist on her or his own institutional picture archiving and communications system viewer. Involvement progression was classified by using a semiquantitative scale from 1 to 4 as the absence of ground-glass opacities (GGOs) and consolidations (score of 1), the presence of GGOs alone (score of 2), the combination of GGOs and consolidations (score of 3), or the presence of consolidations alone (score of 4). The extent of disease was classified as proposed by

Bernheim et al (17): 0% (absent, category 0), 1–25% (minimal, category 1), 26–50% (mild, category 2), 51–75% (moderate, category 3), or over 75% (severe, category 4). The presence of a crazy-paving pattern, mediastinal lymphadenopathy (ie, the presence of at least one lymph node with short axis >10 mm) (22), and pleural effusion was also recorded.

The skeletal muscle area was measured by using the picture archiving and communications system viewer tools of each hospital. As previously reported (7,23), axial CT images at the T5 and T12 vertebral levels were chosen to measure the electronic attenuation expressed in Hounsfield units and the cross-sectional areas of the paravertebral SMM on both sides of the spine, including the SMM of the erector spinae muscle, longissimus thoracis muscle, spinalis thoracis muscle, and iliocostalis lumborum muscle (7,24). To remove the effect of arm-related noise due to the potential position of the upper arms along the patient's sides, we normalized SMM attenuation values by measuring aortic blood attenuation at the T5 and T12 levels.

Because direct measurements of height and weight were not available for all patients, we used the vertebral size as a proxy of the body mass index for SMM indexing (25). Measuring the anteroposterior diameter of the T12 vertebra in an axial section located in the middle of the vertebra, we estimated patients' height and obtained dorsal muscle indexes at T5 and T12 by dividing the SMM at T5 and the SMM at T12 by the anteroposterior T12 vertebral size.

All skeletal muscle measurements and indexes were dichotomized as being over or under the median value of each variable distribution; patients with values over the median were considered to have a normal muscle status, whereas those with values under the median were considered to have lower muscle mass.

Statistical Analysis

Categorical variables were reported as numbers and percentages, and continuous variables were reported as means and standard deviations or as medians and interquartile ranges according to their distribution, as assessed with the Shapiro-Wilk test.

To find potential associations between variables in predicting ICU admission and death during hospitalization, we first used univariate binary logistic regression to calculate unadjusted odds ratios (ORs) with their 95% CIs for each variable. We then aimed to compare the outcome discrimination performance of four different models, with all including sex, age, and body mass index values but with each focusing on a different group of variables. Model 1 considered only clinical variables, model 2 considered only muscle status, model 3 considered muscle status and chest CT features, and model 4 considered clinical variables, muscle status, and chest CT features. A confirmatory model that solely focused on chest CT features was also built to enable the comparison of the relative contributions of chest CT features and muscle status to the outcome discrimination performance (Tables E7, E8; Figs E1, E2 [all online]). Variable selection for model building was performed by using multivariable linear regression (backward elimination) after data imputation for missing values was performed (mean replacement for continuous variables and nearest-neighbor imputation for categorical variables after random missingness hypothesis verification). Selected variables entered multivariable binary logistic regression, and adjusted ORs and their 95% CIs were calculated. The performance of the obtained models in predicting outcomes was assessed by using receiver operating characteristic curve analysis and area under the receiver operating characteristic curve (AUC) evaluation, with AUCs being compared by using the DeLong method (26).

Analyses were performed using SPSS (version 26.0; IBM), and *P* values less than .05 were considered to indicate statistical significance.

Results

Among 564 patients with chest CT performed within 24 hours of admission to the four centers, 12 (2%) were excluded because their CT examinations had inadequate image quality, whereas no patients were excluded for diseases known to chronically impair the muscular status (Fig 1). As detailed in Table 1, a total of 552 patients from the four centers were therefore included in this study: 270 of 552 (49%) from center 1, 197 of 552 (36%) from center 2, 54 of 552 (10%) from center 3, and 31 of 552 (6%) from center 4. Among these 552 patients, 364 of 552 (66%) were men and 188 of 552 (34%) were women, and patients had an overall median age of 65 years (interquartile range, 54–75 years). Patients were admitted to one of the four hospitals from February 21, 2020, to April 30, 2020 (ie, during the first COVID-19 pandemic peak in Northern Italy). The median hospitalization length was 7 days (interquartile range, 5–13 days), and 92 of 552 patients (17%) were admitted to the ICU during their hospital stay. For outcome assessment, censoring was applied on June 1, 2020, when all 552 patients had either been discharged (445 of 552 patients, 81%) or had died during hospitalization (107 of 552 patients, 19%).

At emergency department admission, fever was the most common symptom, affecting 437 of 552 patients (79%), which was followed in prevalence by cough (318 of 552 patients, 58%) and dyspnea (244 of 552 patients, 44%). At least one comorbidity was found in 333 of 552 patients (60%), with cardiovascular diseases being the most frequent (271 of 552 patients, 49%), which was followed in prevalence by diabetes (98 of 552 patients, 18%). The overall median estimated height was 1.70 m (interquartile range, 1.61–1.76 m). Weight was available for 138 of 552 patients (median, 80 kg [interquartile range, 70–90 kg]), whereas a direct recording or calculation of the body mass index was available for 201 of 552 patients (median, 26 kg/m^2 [interquartile range, 24–30 kg/m^2]; the normal body mass index range for our population is 18.5–25 kg/m^2). Laboratory test results were available in all patients, with a median white blood cell count of 6.0 × 10^3/μl (interquartile range, 4.5–8.2 × 10^3/μl; reference range, 4–11 × 10^3/μl), a median lymphocyte count of 1.1 × 10^3/μl (interquartile range, 0.8–1.4 × 10^3/μl; reference range, 1–5 × 10^3/μl), and a median platelet count of 185 × 10^3/μl (interquartile range, 147–236 × 10^3/μl; reference range, 150–450 × 10^3/μl).

CT Findings

At chest CT performed at emergency department admission, parenchymal involvement had progressed only to GGOs without

Table 1: Demographics, Comorbidities, and Imaging Characteristics

Parameter	Finding
Demographics	
Sex (men/women)	364/188
Median age (y)*	65 (53–73)
No. with comorbidities at emergency department admission	
Cardiovascular diseases	271 (49.1)
Diabetes	98 (17.8)
Chronic obstructive pulmonary disease	46 (8.3)
Previous neurologic disease	22 (4.0)
Oncologic history	48 (8.7)
Chronic kidney disease	32 (5.8)
CT findings and metrics	
Lung and thorax	
Median progression of parenchymal involvement*†	3 (2–3)
Median extent of parenchymal involvement*‡	2 (2–3)
No. with bilateral parenchymal involvement	467 (84.6)
No. with crazy-paving pattern	200 (36.2)
No. with pleural effusion	39 (7.1)
Mediastinal lymphadenopathy	87 (15.8)
Skeletal muscles*	
Median SMM_{T5} (mm^2)	1940 (1208–3189)
Median HU_{T5}	23 (12–32)
Median DMI_{T5} (cm^2/m^2)	6.6 (4.3–11.2)
Median SMM_{T12} (mm^2)	3100 (2499–3796)
Median HU_{T12}	37 (24–47)
Median DMI_{T12} (cm^2/m^2)	10.8 (8.9–12.8)
Hospital stay and outcomes	
Median hospitalization length (d)*	7 (5–13)
No. of patients admitted to intensive care unit	92 (16.7)
No. of deceased patients	107 (19.4)

Note.—Unless otherwise specified, data are numbers with percentages in parentheses. DMI_{T12} = dorsal muscle index at T12, DMI_{T5} = dorsal muscle index at T5, HU_{T12} = paravertebral muscle attenuation at T12 in Hounsfield units, HU_{T5} = paravertebral muscle attenuation at T5 in Hounsfield units, SMM_{T12} = skeletal muscle mass at T12, SMM_{T5} = skeletal muscle mass at T5.

* Data in parentheses are the interquartile range.

† Scores are as follows: 1, absence both of ground-glass opacities and of consolidations; 2, presence of ground-glass opacities only; 3, combination of ground-glass opacities and consolidations; and 4, presence of consolidations only.

‡ The semiquantitative categories from 0 to 4, as described by Bernheim et al. are as follows: 0, 0% extension; 1, 1–25% extension; 2, 26–50% extension; 3, 51–75% extension; and 4, over 75% extension. Source.—Reference 17.

consolidations in 172 of 552 patients (31%), had progressed to GGOs with consolidations in 315 of 552 (57%) patients, and had progressed to consolidations without GGOs in 13 of 552 patients (2%). A minimal extent of parenchymal involvement was found in 133 of 552 (24%) patients, mild parenchymal involvement was found in 146 of 552 (26%) patients, moderate parenchymal involvement was found in 158 of 552 (29%) patients, and severe parenchymal involvement was found in 104 of 552 (19%) patients. Other lung parenchymal, chest, and skeletal muscle features are detailed in Table 1. Two examples of patients for whom very low SMM at T5 and SMM at T12 paravertebral values contributed to the prediction of ICU admission and death are depicted in Figure 2 and Figure 3, respectively.

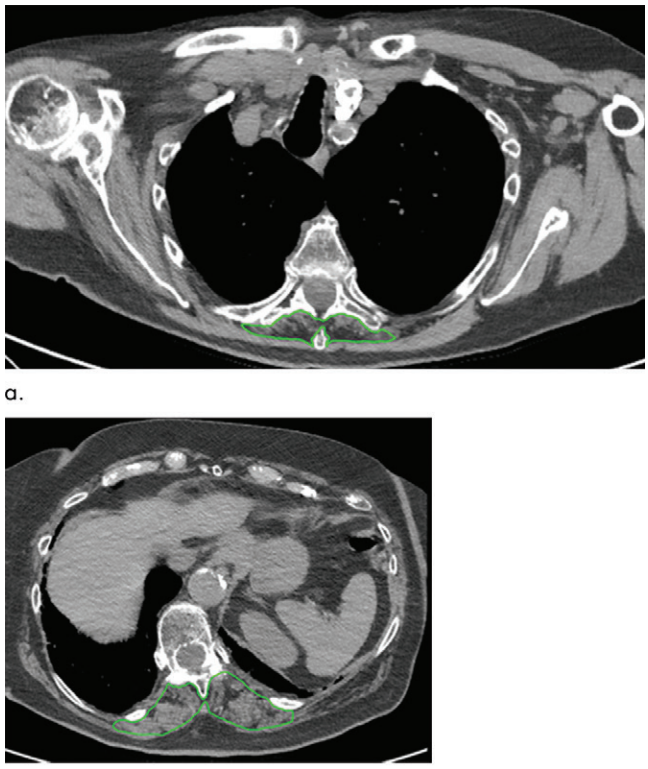

Figure 2: Example of severely impaired muscle status with subsequent intensive care unit admission. Skeletal muscle area segmentation on chest CT images in a 79-year-old woman with COVID-19 obtained at **(a)** T5 level and **(b)** T12 level is shown. This patient presents with fever, cough, mild bilateral lung parenchymal involvement (category 2, according to Bernheim et al [17]), coexisting ground-glass opacities and consolidations and no evidence of crazy paving, pleural effusion, or mediastinal lymphadenopathy. She has no comorbidities and no abnormalities in laboratory test results considered (white blood cell count, lymphocyte count, platelet count). Muscle status parameters are, however, all impaired, save for dorsal muscle index at T12. T5 paravertebral muscle area (890 mm^2), T5 paravertebral muscle attenuation (8 HU), T5 dorsal muscle index (6.6 cm^2/m^2), T12 paravertebral muscle area (2440 mm^2), and T12 paravertebral muscle attenuation (5 HU) are all in the lowest quartile of their overall distributions.

Regression Analyses

Unadjusted ORs for ICU admission and death from univariate binary logistic regression are presented for each variable in the first columns of Table 2 and Table 3, respectively. The details of model building through multivariable linear regression are shown in Tables E3–E6 (online); variables selected by backward elimination entered multivariable binary logistic regression, and adjusted ORs for the four predictive models for ICU admission (Table 2) and the four predictive models for death (Table 3) were

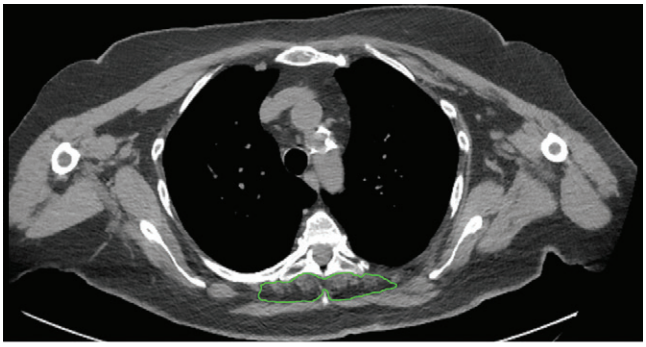

a.

b.

Figure 3: Example of severely impaired muscle status with subsequent intensive care unit admission and death. Skeletal muscle area segmentation on chest CT images in a 62-year-old woman with COVID-19 at **(a)** T5 level and **(b)** T12 level. This patient presents with fever, dyspnea, mild bilateral lung parenchymal involvement (category 2, according to Bernheim et al [17]), consolidations without ground-glass opacities, and no evidence of crazy paving, pleural effusion, or mediastinal lymphadenopathy. She has previous history of cardiovascular comorbidities, diabetes, and class I obesity. All considered laboratory test results (white blood cell count, lymphocyte count, platelet count) are within normal ranges. Muscle status parameters were, however, all impaired. T5 paravertebral muscle area (750 mm^2), T5 paravertebral muscle attenuation (10 HU), T5 dorsal muscle index (2.9 cm^2/m^2), T12 paravertebral muscle area (2300 mm^2), T12 paravertebral muscle attenuation (5 HU), and T12 dorsal muscle index (6.7 cm^2/m^2) are all in the lowest quartile of their overall distributions, with marked fatty degeneration at both T5 and T12.

calculated. Among muscle status parameters, multivariable linear regression selected paravertebral SMM at T5 and SMM at T12 as predictors of ICU admission and death in all models involving muscle status (model 2, model 3, and model 4). At multivariable logistic regression on model 3 (muscle status and chest CT features), paravertebral SMM at T5 had the highest statistically significant OR for both ICU admission (OR, 4.8; 95% CI: 2.7, 8.5; $P < .001$) and death (OR, 2.3; 95% CI: 1.0, 2.9; $P = .03$). These findings were mirrored in model 4 (clinical variables, muscle status, and chest CT features), in which paravertebral SMM at T5 also had the highest statistically significant OR for both ICU admission (OR, 4.3; 95% CI: 2.5, 7.7; $P < .001$) and death (OR, 2.3; 95% CI: 1.3, 3.7; $P = .001$).

Among models considering only a category of features, receiver operating characteristic analysis for the prediction of ICU admission (Fig 4) resulted in an AUC of 0.74 (95% CI: 0.68, 0.79; $P < .001$) for model 1 and an AUC of 0.70 (95% CI: 0.64, 0.76; $P < .001$) for model 2, whereas among combined models, an AUC of 0.83 was obtained for model 3 (95% CI: 0.78, 0.87; $P < .001$) and an AUC of 0.83 was obtained for model 4 (95% CI: 0.79, 0.88; $P < .001$). The AUC comparison showed no significant differences between the AUCs of model 1 and model 2 ($P = .22$), whose performances were, however, significantly inferior to those of model 3 and model 4 ($P < .001$). No significant difference was found between the AUCs of model 3 and model 4 ($P = .38$).

Receiver operating characteristic analysis for the prediction of death (Fig 5) among models considering only a category of features resulted in an AUC of 0.80 (95% CI: 0.75, 0.84; $P < .001$) for model 1 and an AUC of 0.79 (95% CI: 0.75, 0.83; $P < .001$) for model 2, whereas among models, an AUC of 0.86 was obtained for model 3 (95% CI: 0.83, 0.90; $P < .001$) and an AUC of 0.87 was obtained for model 4 (95% CI: 0.84, 0.91; $P < .001$). The AUC comparison showed no significant differences between model 1 and model 2 ($P = .60$), whose performances were, however, significantly inferior to those of model 3 and model 4 ($P < .001$), between which no significant difference was detected ($P = .28$).

Discussion

In this retrospective multicenter study on the prognostic role of lower muscle mass in patients with COVID-19, we evaluated 552 patients from four institutions in Northern Italy that admitted and treated patients during the first COVID-19 pandemic peak between February 21 and April 30, 2020. Our main finding was the association between a lower-than-median paravertebral muscle mass measured on chest CT images obtained at admission and adverse outcomes of patients with COVID-19 during the first pandemic peak. In multivariable logistic regression models considering clinical variables, chest CT features, and muscle status, a lower-than-median paravertebral muscle area at the T5 level yielded the highest odds ratios for intensive care unit admission (4.3; $P < .001$) and death (2.3; $P = .001$). A model combining CT-derived muscle status and the extent of lung disease enabled the prediction of death (area under the receiver operating characteristic curve, 0.86) without any increase in performance occurring with the addition of clinical data.

In patients with COVID-19, advanced age and various preexisting comorbidities have been associated with a higher risk of death (1,2,21,27,28). Although the same has been documented for pulmonary parenchymal damage and associated pathologic features assessed on chest CT images (19,22,29), to our knowledge few articles have investigated whether sarcopenia and lower muscle mass are negative predictors for severe COVID-19 (12–14). Nevertheless, impaired muscle status has long been associated with higher mortality risk in critical care: sarcopenia and lower muscle mass, detected by using CT, are primary predictors of worse outcomes in mechanically ventilated patients (30–32).

Our study confirmed the negative prognostic role played in patients with COVID-19 by age, comorbidities, and some of the chest CT features already recognized as adverse outcome predictors (27). Furthermore, we extended such prognostic evaluation to include impaired muscle status, which proved in our study to be the strongest CT-derived independent predictor of both ICU admission and death. Lower muscle mass probably impacts respiratory muscle function, as do other mechanisms involving

Table 2: Prediction Models for Risk of Intensive Care Unit Admission (n = 92) for Hospitalized Patients with COVID-19

			Model 1: Clinical Variables*		Model 2: Muscle Status*		Model 3: Muscle Status and Chest CT Features*		Model 4: Clinical Variables, Muscle Status, Chest CT Features*	
Variable	Unadjusted OR	*P* Value	Adjusted OR	*P* Value	Adjusted OR	*P* Value	Adjusted OR	*P* Value	Adjusted OR	*P* Value
Male sex	2.6 (1.5, 4.6)	.001	2.6 (1.4, 4.6)	.001	2.5 (1.3, 4.5)	.001	1.9 (1.1, 3.6)	.02	2.0 (1.1, 3.7)	.02
Age	0.99 (0.98, 1.00)	.16	…	…	…	…	…	…	…	…
Lung involvement progression	1.1 (0.7, 1.6)	.77	…	…	…	…	…	…	…	…
Crazy paving	1.7 (1.1, 2.8)	.02	…	…	…	…	…	…	…	…
Bilateral lung involvement	31 (1, 744)	.04	…	…	…	…	40 (1, 3119)	.10	60 (0, 8931)	.11
Lung involvement extent	1.5 (1.2, 1.9)	<.001	…	…	…	…	1.7 (1.3, 2.8)	<.001	1.9 (1.5, 2.5)	<.001
Pleural effusion	2.1 (1.0, 4.6)	.05	…	…	…	…	…	…	…	…
Mediastinal lymphadenopathy	1.3 (0.7, 2.4)	.40	…	…	…	…	…	…	…	…
SMM_{T5}	3.4 (2.1, 5.6)	<.001	…	…	3.3 (2.0, 5.5)	<.001	4.8 (2.7, 8.5)	<.001	4.3 (2.5, 7.7)	<.001
DMI_{T5}	3.0 (1.8, 4.9)	<.001	…	…	…	…	…	…	…	…
HU_{T5}	1.0 (0.6, 1.6)	>.99	…	…	…	…	…	…	…	…
SMM_{T12}	1.3 (0.8, 2.0)	.29	…	…	1.9 (1.5, 2.4)	.04	1.5 (1.0, 1.8)	.08	2.0 (0.8, 3.2)	.07
DMI_{T12}	0.7 (0.4, 1.1)	.09	…	…	…	…	…	…	…	…
HU_{T12}	1.2 (0.7, 1.8)	.49	…	…	…	…	…	…	…	…
Cardiovascular diseases	1.2 (0.7, 1.9)	.47	…	…	…	…	…	…	…	…
Diabetes	1.7 (1.0, 2.9)	.049	1.9 (1.1, 3.4)	.03	…	…	…	…	…	…
COPD	1.5 (0.6, 3.7)	.36	…	…	…	…	…	…	…	…
Neurologic history	1.1 (0.3, 4.1)	.83	…	…	…	…	…	…	…	…
Oncologic history	1.2 (0.5, 2.5)	.69	1.0 (1.00, 1.6)	.02	…	…	…	…	1.4 (1.0, 1.6)	.02
CKD	1.4 (0.6, 3.4)	.42	2.0 (1.0, 3.1)	.06	…	…	…	…	1.7 (1.0, 2.0)	.046
Body mass index	1.1 (1.0, 1.2)	.01	1.11 (1.03, 1.20)	.007	…	…	…	…	…	…
WBC	1.14 (1.07, 1.21)	<.001	1.1 (1.0, 1.2)	.003	…	…	…	…	…	…
Lymphocyte count	1.0 (0.9, 1.3)	.75	…	…	…	…	…	…	…	…
Platelets	1.00 (0.99, 1.00)	.87	…	…	…	…	…	…	…	…

Note.—Data in parentheses are 95% CIs. CKD = chronic kidney disease, COPD = chronic obstructive pulmonary disease, DMI_{T12} = dorsal muscle index at T12, DMI_{T5} = dorsal muscle index at T5, HU_{T12} = paravertebral muscle attenuation at T12 in Hounsfield units, HU_{T5} = paravertebral muscle attenuation at T5 in Hounsfield units, OR = odds ratio, SMM_{T12} = skeletal muscle mass at T12, SMM_{T5} = skeletal muscle mass at T5, WBC = white blood cell count.

* Variables selected through multivariable linear regression with backward elimination (see Tables E3–E6 [online]).

global sarcopenia (12–14), such as the sarcopenia-induced proinflammatory profile (28), that interacts with the cytokine storm triggered by severe SARS-CoV-2 infection (33,34), the prolonged immobilization during hospitalization, and mechanical ventilation (12–14).

If a strong association between lower muscle mass and worse outcomes in patients with COVID-19 is confirmed by further studies, then the role of chest CT could be expanded from use in triage and monitoring to use in prognosis prediction. Because chest CT is effectively used to help detect and stage COVID-19 pneumonia (15,18–20), CT examinations could also be used to identify patients with lower muscle mass who are at higher risk of worse outcomes, therefore enabling simultaneous diagnostic and prognostic assessment to be achieved. Our study showed how the prognostic performance of a model relying only on chest CT–derived features (lung parenchyma and muscle status) is equal to that of one of the models also including clinical variables, which, it should be noted, are relatively more difficult and time-consuming to retrieve. The application of artificial intelligence to both lung and muscle status assessment of chest CT images could further curtail the time needed to obtain such prognostic information, as this approach has already been proposed for muscle status assessment on abdominal CT scans (35).

Table 3: Prediction Models for Risk of Death (n = 107) for Hospitalized Patients with COVID-19

			Model 1: Clinical Variables*		Model 2: Muscle Status*		Model 3: Muscle Status and Chest CT Features*		Model 4: Clinical Variables, Muscle Status, Chest CT Features*	
Variable	Unadjusted OR	*P* Value	Adjusted OR	*P* Value	Adjusted OR	*P* Value	Adjusted OR	*P* Value	Adjusted OR	*P* Value
Male sex	1.9 (1.2, 3.1)	.01	2.7 (1.5, 4.7)	<.001	1.4 (1.0, 2.1)	.01	1.9 (1.1, 3.2)	.02	2.0 (1.2, 3.5)	.009
Age	1.08 (1.06, 1.10)	<.001	1.07 (1.05, 1.10)	<.001	…	…	…	…	…	…
Lung involvement progression	0.9 (0.6, 1.3)	.63	…	…	…	…	…	…	…	…
Crazy paving	1.7 (1.1, 2.7)	.02	…	…	…	…	1.4 (0.9, 2.3)	.11	1.5 (0.9, 2.4)	.11
Bilateral lung involvement	2.4 (0.9, 6.6)	.08	…	…	…	…	…	…	…	…
Lung involvement extent	1.4 (1.2, 1.8)	.001	…	…	…	…	1.4 (1.1, 1.8)	.002	1.4 (1.1, 1.7)	.008
Pleural effusion	3.0 (1.5, 6.1)	.002	…	…	…	…	…	…	…	…
Mediastinal lymphadenopathy	1.9 (1.1, 3.3)	.03	…	…	…	…	…	…	…	…
SMM_{T5}	1.3 (0.8, 2.0)	.25	…	…	2.2 (1.3, 3.7)	.003	2.3 (1.0, 2.9)	.03	2.3 (1.3, 3.7)	.03
DMI_{T5}	1.2 (0.8, 1.8)	.48	…	…	…	…	…	…	…	…
HU_{T5}	0.7 (0.5, 1.1)	.16	…	…	…	…	…	…	…	…
SMM_{T12}	1.4 (0.9, 2.1)	.16	…	…	1.6 (0.9, 2.0)	.03	1.4 (0.9, 2.0)	.04	1.7 (0.9, 2.2)	.048
DMI_{T12}	0.8 (0.5, 1.2)	.27	…	…	…	…	…	…	…	…
HU_{T12}	0.5 (0.3, 0.8)	.002	…	…	…	…	…	…	…	…
Cardiovascular diseases	3.2 (2.0, 5.1)	<.001	1.4 (0.9, 2.5)	.14	…	…	…	…	2.1 (1.2, 4.8)	<.001
Diabetes	2.0 (1.2, 3.3)	.005	2.0 (1.0, 2.5)	.21	…	…	…	…	…	…
COPD	2.1 (1.1, 4.1)	.02	2.0 (0.9, 4.1)	.02	…	…	…	…	2.2 (1.2, 5.1)	.009
Neurologic history	2.1 (0.8, 5.4)	.13	…	…	…	…	…	…	…	…
Oncologic history	1.9 (1.0, 3.7)	.049	…	…	…	…	…	…	…	…
CKD	1.4 (0.6, 3.2)	.41	2.1 (0.9, 5.0)	.08	…	…	…	…	1.6 (1.1, 5.8)	.02
Body mass index	0.94 (0.87, 1.02)	.13	…	…	…	…	…	…	…	…
WBC	1.08 (1.02, 1.15)	.01	1.1 (1.0, 1.2)	.005	…	…	…	…	…	…
Lymphocyte count	1.0 (0.8, 1.2)	.76	…	…	…	…	…	…	…	…
Platelets	1.00 (0.99, 1.00)	.09	…	…	…	…	…	…	…	…

Note.— Data in parentheses are 95% CIs. CKD = chronic kidney disease, COPD = chronic obstructive pulmonary disease, DMI_{T12} = dorsal muscle index at T12, DMI_{T5} = dorsal muscle index at T5, HU_{T12} = paravertebral muscle attenuation at T12 in Hounsfield units, HU_{T5} = paravertebral muscle attenuation at T5 in Hounsfield units, OR = odds ratio, SMM_{T12} = skeletal muscle mass at T12, SMM_{T5} = skeletal muscle mass at T5, WBC = white blood cell count.

* Variables selected through multivariable linear regression with backward elimination (see Tables E3–E6 [online]).

Some limitations of our study, other than its retrospective nature, should be considered. First, these results were obtained during a pandemic peak, characterized by a high disease prevalence and severity. Therefore, the prognostic role of sarcopenia in patients with COVID-19 must be verified during different study periods with lower disease prevalence and/or severity while also considering that effective therapies have been introduced. Second, from a technical point of view, arm-related noise due to the position of the upper arms along a patient's sides could have affected the attenuation values of paravertebral muscles. This could partly justify the absent association of low muscle density with worse outcomes, although we tried to remove this effect by normalizing paravertebral muscle attenuation values by using aortic values. Because a correlation between skeletal muscle

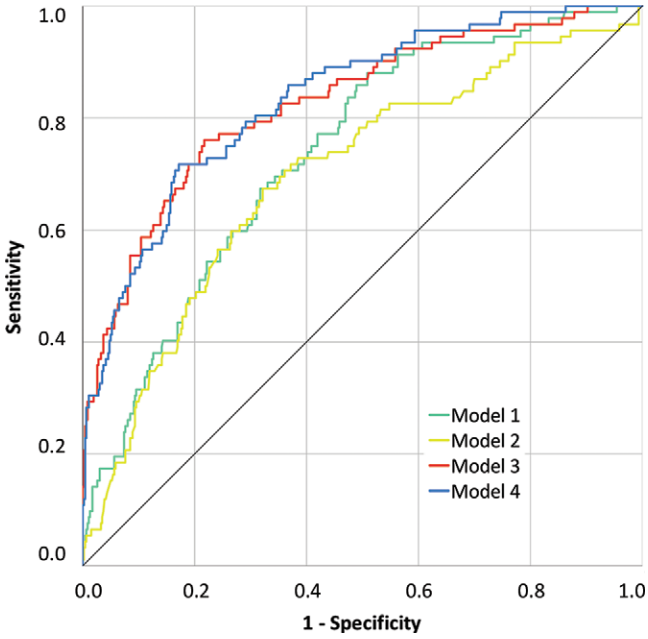

Figure 4: Graph shows receiver operating characteristic curve analysis for prediction of intensive care unit admission. After area under the receiver operating characteristic curve (AUC) comparison by using DeLong method is performed, discrimination performance of model 1 (clinical variables; AUC, 0.74; 95% CI: 0.68, 0.79; $P < .001$) does not significantly differ from that of model 2 (muscle status; AUC, 0.70; 95% CI: 0.64, 0.76; $P < .001$; AUC comparison for model 1 vs model 2, $P = .22$), nor does performance of model 3 (muscle status and chest CT features; AUC, 0.83; 95% CI: 0.78, 0.8; $P < .001$) significantly differ from that of model 4 (clinical variables, muscle status, and chest CT features; AUC, 0.83; 95% CI: 0.79, 0.88; $P < .001$; AUC comparison vs model 3, $P = .38$). However, as depicted, discrimination performance of model 1 and discrimination performance of model 2 are both significantly inferior to those of model 3 and model 4 (all AUC comparisons, $P < .001$).

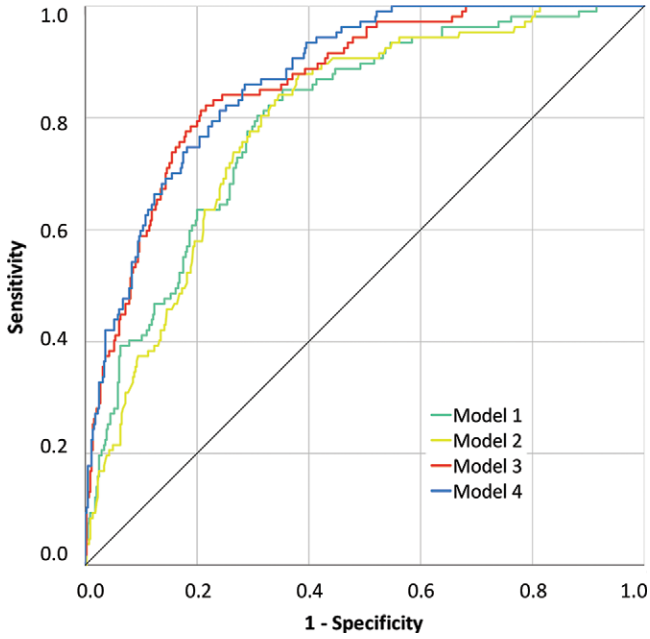

Figure 5: Graph shows receiver operating characteristic curve analysis for prediction of death during hospitalization. After area under the receiver operating characteristic curve (AUC) comparison is performed by using DeLong method, discrimination performance of model 1 (clinical variables; AUC, 0.80; 95% CI: 0.75, 0.84; $P < .001$) does not significantly differ from that of model 2 (muscle status; AUC, 0.79; 95% CI: 0.75, 0.83; $P < .001$; AUC comparison for model 1 vs model 2, $P = .60$), nor does performance of model 3 (muscle status and chest CT features; AUC, 0.86, 95% CI: 0.83, 0.90; $P < .001$) differ from that of model 4 (clinical variables, muscle status, and chest CT features; AUC, 0.87; 95% CI: 0.84, 0.91: $P < .001$; AUC comparison vs model 3, $P = .28$). However, as depicted, discrimination performance of model 1 and discrimination performance of model 2 are both significantly inferior to those of model 3 and model 4 (all AUC comparisons: $P < .001$).

density and mortality in mechanically ventilated patients has been previously reported (31), this point deserves further investigation. Third, height was not available for all patients; thus, we had to estimate the height of some of our patients by using the anteroposterior diameter of the T12 vertebra, an approach that has been previously validated (25). Fourth, our study retrieved data from multiple centers with different CT acquisition parameters and potentially different ICU admission criteria for patients with COVID-19. Similarly, image analysis was performed by different readers with different levels of experience, although these analyses were conducted by using standardized criteria. Fifth, pulmonary vascular damage has been progressively recognized as a major influence on the prognosis of COVID-19 (20). Its inclusion could have further refined the performance of our predictive model, but all of our patients were admitted and treated during the first pandemic peak in the first-hit European region at a time when evidence on this issue was still scarce and the routine evaluation of coagulation parameters was far from being implemented.

In conclusion, a chest CT–based combined model integrating muscle status enabled reliable prediction of intensive care unit admission and death in patients with COVID-19 without clinical variables being used, which highlights the need to consider previously overlooked frailty indicators in COVID-19 diagnostic and therapeutic pathways.

Author contributions: Guarantors of integrity of entire study, A. Carriero, F. Sardanelli, L.M.S.; study concepts/study design or data acquisition or data analysis/interpretation, all authors; manuscript drafting or manuscript revision for important intellectual content, all authors; approval of final version of submitted manuscript, all authors; agrees to ensure any questions related to the work are appropriately resolved, all authors; literature research, S.S., D.A., A. Cozzi, C.M., F. Sardanelli, L.M.S.; clinical studies, S.S., A. Cozzi, C.M., R.A., C.B., S.C., P.S.C.D., E.D., C.D.B., Z.F., S.G., A.E.M., G.M., L.M., A.P., F. Secchi, A.V., V.T., D.Z., L.M.S.; statistical analysis, S.S., D.A., A. Cozzi, L.M.S.; and manuscript editing, S.S., D.A., A. Cozzi, C.M., F. Sardanelli

Disclosures of Conflicts of Interest: S.S. Activities related to the present article: disclosed no relevant relationships. Activities not related to the present article: service on speakers bureau of General Electric; received travel support from Bracco Imaging. Other relationships: disclosed no relevant relationships. **D.A.** disclosed no relevant relationships. **A. Cozzi** disclosed no relevant relationships. **C.M.** disclosed no relevant relationships. **R.A.** disclosed no relevant relationships. **C.B.** disclosed no relevant relationships. **A.B.** disclosed no relevant relationships. **L.A.C.** disclosed no relevant relationships. **A. Carriero** disclosed no relevant relationships. **S.C.** disclosed no relevant relationships. **P.S.C.D.** disclosed no relevant relationships. **E.D.** disclosed no relevant relationships. **C.D.B.** disclosed no relevant relationships. **G.D.P.** disclosed no relevant relationships. **Z.F.** disclosed no relevant relationships. **S.G.** disclosed no relevant relationships. **A.E.M.** disclosed no relevant relationships. **G.M.** disclosed no relevant relationships. **L.M.** disclosed no relevant relationships. **A.P.** disclosed no relevant relationships. **R.R.** disclosed no relevant relationships. **F. Secchi** disclosed no relevant relationships. **A.V.** disclosed no relevant relationships. **V.T.** disclosed no relevant relationships. **I.V.** disclosed no relevant relationships. **D.Z.** disclosed no relevant relationships. **F. Sardanelli** Activities related to the present article: disclosed no relevant relationships. Activities not related to the present article: is board member of and receives payment for lectures including service on speakers bureaus from Bracco Imaging, Bayer Healthcare, and General Electric. Other relationships: is author/editor of books in the radiology field with Springer and EDRA. **L.M.S.** Activities related to

the present article: disclosed no relevant relationships. Activities not related to the present article: is board member of Pfizer; receives payment for lectures including service on speakers bureaus from Abiogen, Fidia Pharma Group, and Novartis; received payment for travel/accommodations/meeting expenses unrelated to activities listed from Bracco Imaging, Samsung, and Abiogen. Other relationships: disclosed no relevant relationships.

References

1. Verity R, Okell LC, Dorigatti I, et al. Estimates of the severity of coronavirus disease 2019: a model-based analysis. Lancet Infect Dis 2020;20(6):669–677.
2. Guo T, Shen Q, Guo W, et al. Clinical characteristics of elderly patients with COVID-19 in Hunan Province, China: a multicenter, retrospective study. Gerontology 2020;66(5):467–475.
3. Calvani R, Marini F, Cesari M, et al. Biomarkers for physical frailty and sarcopenia: state of the science and future developments. J Cachexia Sarcopenia Muscle 2015;6(4):278–286.
4. Albano D, Messina C, Vitale J, Sconfienza LM. Imaging of sarcopenia: old evidence and new insights. Eur Radiol 2020;30(4):2199–2208.
5. Boutin RD, Katz JR, Chaudhari AJ, et al. Association of adipose tissue and skeletal muscle metrics with overall survival and postoperative complications in soft tissue sarcoma patients: an opportunistic study using computed tomography. Quant Imaging Med Surg 2020;10(8):1580–1589.
6. Giraudo C, Cavaliere A, Lupi A, Guglielmi G, Quaia E. Established paths and new avenues: a review of the main radiological techniques for investigating sarcopenia. Quant Imaging Med Surg 2020;10(8):1602–1613.
7. Troschel AS, Troschel FM, Best TD, et al. Computed tomography-based body composition analysis and its role in lung cancer care. J Thorac Imaging 2020;35(2):91–100.
8. Okazaki T, Ebihara S, Mori T, Izumi S, Ebihara T. Association between sarcopenia and pneumonia in older people. Geriatr Gerontol Int 2020;20(1):7–13.
9. Maeda K, Akagi J. Muscle mass loss is a potential predictor of 90-day mortality in older adults with aspiration pneumonia. J Am Geriatr Soc 2017;65(1):e18–e22.
10. Buchman AS, Boyle PA, Wilson RS, Gu L, Bienias JL, Bennett DA. Pulmonary function, muscle strength and mortality in old age. Mech Ageing Dev 2008;129(11):625–631.
11. de Siqueira JVV, Almeida LG, Zica BO, Brum IB, Barceló A, de Siqueira Galil AG. Impact of obesity on hospitalizations and mortality, due to COVID-19: a systematic review. Obes Res Clin Pract 2020;14(5):398–403.
12. Ekiz T, Kara M, Özcan F, Ricci V, Özçakar L. Sarcopenia and COVID-19: a manifold insight on hypertension and the renin angiotensin system. Am J Phys Med Rehabil 2020;99(10):880–882.
13. Ufuk F, Demirci M, Sagtas E, Akbudak IH, Ugurlu E, Sari T. The prognostic value of pneumonia severity score and pectoralis muscle area on chest CT in adult COVID-19 patients. Eur J Radiol 2020;131:109271.
14. Kottlors J, Zopfs D, Fervers P, et al. Body composition on low dose chest CT is a significant predictor of poor clinical outcome in COVID-19 disease: a multicenter feasibility study. Eur J Radiol 2020;132:109274.
15. Rubin GD, Ryerson CJ, Haramati LB, et al. The role of chest imaging in patient management during the COVID-19 pandemic: a multinational consensus statement from the Fleischner Society. Radiology 2020;296(1):172–180.
16. Sverzellati N, Milanese G, Milone F, Balbi M, Ledda RE, Silva M. Integrated radiologic algorithm for COVID-19 pandemic. J Thorac Imaging 2020;35(4):228–233.
17. Bernheim A, Mei X, Huang M, et al. Chest CT findings in coronavirus disease-19 (COVID-19): relationship to duration of infection. Radiology 2020;295(3):200463.
18. Falaschi Z, Danna PSC, Arioli R, et al. Chest CT accuracy in diagnosing COVID-19 during the peak of the Italian epidemic: a retrospective correlation with RT-PCR testing and analysis of discordant cases. Eur J Radiol 2020;130:109192.
19. Colombi D, Bodini FC, Petrini M, et al. Well-aerated lung on admitting chest CT to predict adverse outcome in COVID-19 pneumonia. Radiology 2020;296(2):E86–E96.
20. Spagnolo P, Cozzi A, Foà RA, et al. CT-derived pulmonary vascular metrics and clinical outcome in COVID-19 patients. Quant Imaging Med Surg 2020;10(6):1325–1333.
21. Evidence used to update the list of underlying medical conditions that increase a person's risk of severe illness from COVID-19. Centers for Disease Control and Prevention Web site. https://www.cdc.gov/coronavirus/2019-ncov/need-extra-precautions/evidence-table.html. Published 2020. Accessed February 19, 2021.
22. Sardanelli F, Cozzi A, Monfardini L, et al. Association of mediastinal lymphadenopathy with COVID-19 prognosis. Lancet Infect Dis 2020;20(11):1230–1231.
23. Nishimura JM, Ansari AZ, D'Souza DM, Moffatt-Bruce SD, Merritt RE, Kneuertz PJ. Computed tomography-assessed skeletal muscle mass as a predictor of outcomes in lung cancer surgery. Ann Thorac Surg 2019;108(5):1555–1564.
24. Hua X, Deng J-P, Long ZQ, et al. Prognostic significance of the skeletal muscle index and an inflammation biomarker in patients with breast cancer who underwent postoperative adjuvant radiotherapy. Curr Probl Cancer 2020;44(2):100513.
25. Waduud MA, Sucharitkul PPJ, Drozd M, Gupta A, Hammond C, Ashbridge Scott DJ. Validation of two-dimensional vertebral body parameters in estimating patient height in elderly patients. Br J Radiol 2019;92(1104):20190342.
26. DeLong ER, DeLong DM, Clarke-Pearson DL. Comparing the areas under two or more correlated receiver operating characteristic curves: a nonparametric approach. Biometrics 1988;44(3):837–845.
27. Altmayer S, Zanon M, Pacini GS, et al. Comparison of the computed tomography findings in COVID-19 and other viral pneumonia in immunocompetent adults: a systematic review and meta-analysis. Eur Radiol 2020;30(12):6485–6496.
28. Boreskie KF, Hay JL, Duhamel TA. Preventing frailty progression during the COVID-19 pandemic. J Frailty Aging 2020;9(3):130–131.
29. Cesari M, Proietti M. COVID-19 in Italy: ageism and decision making in a pandemic. J Am Med Dir Assoc 2020;21(5):576–577.
30. Weijs PJ, Looijaard WG, Dekker IM, et al. Low skeletal muscle area is a risk factor for mortality in mechanically ventilated critically ill patients. Crit Care 2014;18(2):R12.
31. Looijaard WGPM, Dekker IM, Stapel SN, et al. Skeletal muscle quality as assessed by CT-derived skeletal muscle density is associated with 6-month mortality in mechanically ventilated critically ill patients. Crit Care 2016;20(1):386.
32. Elliott JE, Greising SM, Mantilla CB, Sieck GC. Functional impact of sarcopenia in respiratory muscles. Respir Physiol Neurobiol 2016;226:137–146.
33. Mehta P, McAuley DF, Brown M, et al. COVID-19: consider cytokine storm syndromes and immunosuppression. Lancet 2020;395(10229):1033–1034.
34. Li T, Zhang Y, Gong C, et al. Prevalence of malnutrition and analysis of related factors in elderly patients with COVID-19 in Wuhan, China. Eur J Clin Nutr 2020;74(6):871–875.
35. Burns JE, Yao J, Chalhoub D, Chen JJ, Summers RM. A machine learning algorithm to estimate sarcopenia on abdominal CT. Acad Radiol 2020;27(3):311–320.